A Numerical Investigation of the Stability of Isolated Shallow Water Vortices

A. Stegner

Laboratoire de Météorologie Dynamique, École Normale-Supérieure, Paris, France

D. G. Dritschel

Mathematical Institute, University of St. Andrews, North Haugh, St. Andrews, United Kingdom

(Manuscript received 24 March 1999, in final form 29 November 1999)

ABSTRACT

Motivated by observational data and recent numerical simulations showing that ageostrophic effects may play an important role in the dynamics and transport of large-scale vortices in the atmosphere and the oceans, the authors examine the stability of a family of isolated vortices, numerically, using the contour-advective semi-Lagrangian algorithm. The full shallow-water equations (1½-layer model) are integrated in order to investigate vortices over a wide range of parameters. In order to characterize the cyclone–anticyclone asymmetry, the stability of a couple of vortices having velocity profiles of opposite sign is compared. It is found that ageostrophic effects (finite Rossby number) tend to stabilize anticyclones but destabilize cyclones. On the other hand, large-scale effects (small Burger number) are shown to stabilize all vortices for this reduced-gravity model. Here again, the anticyclones tend to be favored in this restabilization process. These results are compared with a linear stability analysis performed in the framework of the standard quasigeostrophic model that predicts a symmetric evolution for cyclones and anticyclones. The authors have shown that a significant departure from QG dynamics, due to ageostrophic and large-scale effects, appears in a range of parameters relevant to large-scale coherent structures in nature.

1. Introduction

Long-lived, large-scale vortices are common features in planetary atmospheres, particulary in those of the outer planets (Smith et al. 1979) and also in the Earth's oceans (Olson 1991). Such vortices are known to greatly influence the transport properties of the global circulation. For instance, a single vortex, or eddy, generated by the Agulhas Current can cross the South Atlantic Ocean carrying an amount of energy equal to 5%–7% of the annual wind input of energy to the large-scale circulation (Olson and Evans 1986). Other oceanic vortices such as meddies (subsurface eddies with a warm and salty core) are known to play an important role in the transport of salt in the northeast Atlantic. This efficient transport mechanism has motivated, over the past few years, a number of theoretical, experimental, and numerical studies of the stability of quasi-two-dimensional vortices. However, these studies have often been limited to a restricted range of parameters, and a global description of the stability of isolated vortices in a sim-

ple model like the shallow-water model is still lacking. Rayleigh's ''inflexion point'' criteria for circular vortices can be readily generalized to balanced models such as the Quasi-Geostrophic (Pedlosky 1987) or the Frontal Geostrophic (Cushman-Roisin 1986). In these cases, circular vortices with a monotonic ''equivalent potential vorticity'' (the truncated potential vorticity of the model) are linearly stable to normal mode pertubations; see Table 1. Other sufficient criteria based on a formal stability analysis of a Hamiltonian system were recently found for these balanced models (Holm 1985; Ben Jelloul and Zeitlin 1999). However, according to these criterion (see Table 1), isolated vortices (having zero net circulation) cannot satisfy formal stability (in the energy norm) in the 2D Euler and QG models. Therefore, nonlinear stability conditions following Arnold's method (Arnold 1978) are not available for isolated vortices in these models. The full nonlinear stability analysis performed for the Frontal Geostrophic model (Ben Jelloul and Zeitlin 1999) leads to a nonlinear stability condition that is not symmetric for cyclones and anticyclones, but vortices of both sign may satisfy it, and a detailed analysis able to distinguish which sign is more stable is not straightforward. Moreover, these balanced models, which were derived from a small Rossby number expansion, do not account for ageostrophic effects. Efforts

Corresponding author address: Dr. Alexandre Stegner, Laboratoire de Météorologie Dynamique, École Normale Supérieure, 24, rue Lhomond, 75005 Paris Cedex, France.
E-mail: stegner@lmd.ens.fr

TABLE 1. Sufficient stability criterion for circular vortices.

	2D Euler	Quasigeostrophic	Frontal geostrophic	Shallow water	
Equivalent PV	$|\omega|$	$|\omega| - \mathrm{Bu}^{-1}h$	$\dfrac{1}{H_o + h}$	$\dfrac{f_o + |\omega|}{H_o + h}$	
Rayleigh stability criterion (normal mode analysis)	Montonic $|\omega|$	Monotonic q	Monotonic h		
Formal stability on energy invariant	$\dfrac{U(r)}{\partial_r|\omega|} > 0$	$\dfrac{U(r)}{\partial_r q} > 0$	Monotonic h	$\dfrac{U(r)}{\partial_r q} > 0, \quad \dfrac{U(r)}{\sqrt{g(H_o + h(r))}} > 1$	
(Hamiltonian formulation)	(Holm et al. 1985)	(Holm et al. 1985)	(Ben Jelloul and Zeitlin 1999)	(Ripa 1987)	

have been made to develop a stability criterion directly within the framework of the shallow-water equations, and a sufficient condition for the stability of circular flows has been derived by Ripa (1987) (see Table 1). However, this condition cannot be satisfied by isolated vortices. Therefore, it appears necessary to resort to laboratory experiments or direct numerical simulations in order to investigate the stability of large-scale isolated structures. Previous numerical simulations (Polvani et al. 1994; Arai and Yamagata 1994) devoted to decaying shallow water turbulence have shown that the departure from quasigeostrophy leads to a significant cyclone–anticyclone asymmetry for which anticyclonic vortices are generally preferred. However, in turbulence many mechanisms may be responsible for this dynamical asymmetry (merging processes, stability, wave–vortex interactions). The role played by ageostrophic effects in the behavior of an isolated vortex is still not well understood. In particular we wish to address the following questions:

- How are the stability properties and lifetime of an isolated vortex affected by ageostrophic and large-scale effects?
- At what Burger and Rossby numbers do departures from the QG model become significant?

We will investigate the stability of the following class of circular vortices parameterised by the vorticity profile "steepness" α:

$$\omega(s) = \epsilon f_o \left(1 - \frac{1}{2}s^\alpha\right) \exp\left(-\frac{s^\alpha}{\alpha}\right), \quad (1.1)$$

where $s = r/L_o$ (N.B. the maximum velocity occurs at $s = 1$), f_o is the Coriolis parameter, and $\epsilon = \omega_{\max}/f_o$ is the dynamical Rossby number. Equation (1) describes a wide range of vorticity profiles having smooth ($1 < \alpha < 2$) or steep gradients (large α). The case $\alpha = 2$ corresponds to a Gaussian velocity profile. All of these vortices are isolated; that is, their circulation vanishes at large radii: this implies that the core vorticity is surrounded by a ring of oppositely signed vorticity. In incompressible two-dimensional flows, the stability of an isolated circular vortex depends only on the shape of the vorticity distribution. For (1) it was shown numer-

ically (Carton et al. 1989) that for $\alpha > \alpha_c = 1.8$–1.9 both cyclones and anticylones are unstable and lead to a tripolar structure, while for $(\alpha - \alpha_c)/\alpha_c \simeq 1$ the initial circular structure splits into two dipoles (Orlandi and van Heijst 1992; Carton and Legras 1994).

The first step to a more realistic dynamical description of geophysical vortices is to use the full shallow-water equations. The height profile of a steady circular vortex satisfies gradient wind balance

$$\frac{v^2}{r} + f_o v = g\frac{\partial h}{\partial r}, \quad (1.2)$$

which takes into account the effect of the centrifugal force in the pressure field. Then the relative amplitude of the height field h/H_o scales as $\epsilon(L_o/R_d)^2$. Here, H_o is the undisturbed layer thickness, L_o is the size of the vortex, and $R_d = \sqrt{gH_o}/f_o$ is the deformation radius. The potential vorticity

$$q = \frac{f_o + \omega}{H_o + h} \quad (1.3)$$

can be expressed as a linear operator on h only if ω and h are respectively small compared to f_o and H_o. Otherwise, the stability of circular vortices may be sensitive to ageostrophic effects (ϵ) and large-scale effects (L_o/R_d). Hence, in addition to the steepness parameter, two more parameters control stability: the Rossby number and the Burger number $\mathrm{Bu} = (R_d/L_o)^2$. Their effect on stability is investigated below.

In the shallow-water model, a cyclone and an anticyclone satisfying (2) cannot have the same velocity, potential vorticity, and height anomalies (same but with opposite signs). Therefore, in order to investigate the cyclone–anticyclone asymmetry, one must choose the sense in which an cyclone and anticyclone are "equivalent." Here we choose the velocity profile; vortices with equal magnitude but opposite-signed velocity are said to be equivalent (such vortices have equal but opposite vorticity). This choice is convenient because the dynamical parameters ϵ and Bu remain invariant to the transformation $v \to -v$ and more reliable comparison with observational data can be made with velocity than with PV or height anomalies.

2. The shallow-water CASL algorithm

The contour-advective semi-Lagrangian (CASL) algorithm (Dritschel and Ambaum 1997; Dritschel et al. 1999) is used to solve the full single-layer shallow-water equations. This algorithm holds the conservative PV field q in contour form to avoid excessive dissipation. If the fluid motion is nearly balanced, both the height h and the divergence δ fields remain smooth and hence decay rapidly with increasing wavenumber. Such a decay permits one to evolve h and δ accurately in spectral space using a moderate resolution (here 128^2 or 256^2) and without any explicit dissipation.

The initial conditions for all of our simulations consist of an axisymmetric vortex discretized into N PV contours. An example of the contour and grid representations used for a continuous circular vortex having a steepness parameter $\alpha = 3$ is shown in Fig. 1. The PV jump at each contour $r = r_j = j\Delta r$ is such that the circulation is identical for the continuous and discrete representation. In other words, the value of the velocity at each PV contour is equal to that at the same location in the continuous representation. We used between 30 and 40 contours in order to obtain a sufficiently close match between the representations; for instance, the linear growth rate converges to within 5%–10% of the value obtained from a QG linear stability analysis of the continuous profile.

We then added small, random, nonaxisymmetric disturbances to stimulate any potential instability (this was done by radial displacements of the contour points). The height and divergence fields were adjusted iteratively so that their second-order time derivatives vanished at $t = 0$. The time evolution was computed using "contour advection" for PV, that is, solving $dx/dt = \mathbf{v}(x, t)$ in place of

$$\partial_t q + \mathbf{v} \cdot \nabla q = 0 \qquad (2.1)$$

and a standard semi-implicit, pseudospectral treatment of the height and divergence equations,

$$\partial_t h + \nabla \cdot (\mathbf{v}h) = 0 \qquad (2.2)$$

$$\partial_t \delta = 2J(u, v) - \nabla \cdot (\mathbf{v}\delta) + f_o \omega - g\Delta h, \qquad (2.3)$$

where $J(a, b)$ is the Jacobian operator. Notably, no explicit dissipation is used for (5) or (6), whereas "surgery" is used to limit the scale of filamentary PV to a tenth of the grid scale. See Dritschel et al. (1999) for all details, including comparisons with standard numerical approaches.

FIG. 1. Contour and grid representations of a continuous circular vortex having a steepness parameter $\alpha_c = 3$ ($L_o = R_d = 0.8$, $H_o = 1$, $f_o = 4\pi$, $\epsilon = 0.1$): (a) potential vorticity, (b) vorticity, and (c) height. The solid line corresponds to the continuous profile while the bold line and scatterplot correspond respectively to the contour and grid discretization.
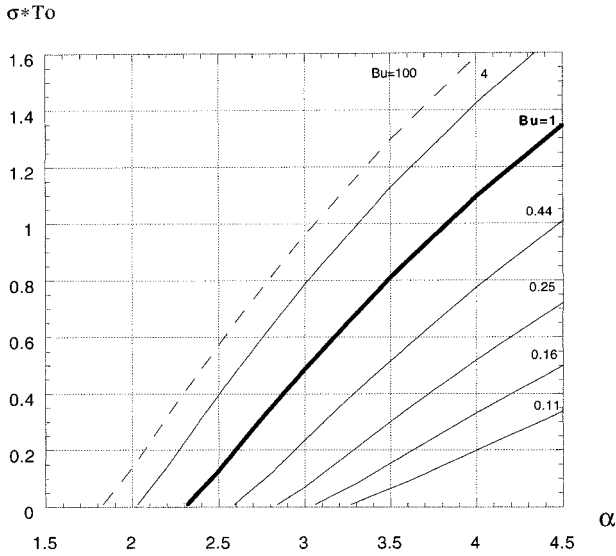
σ*To
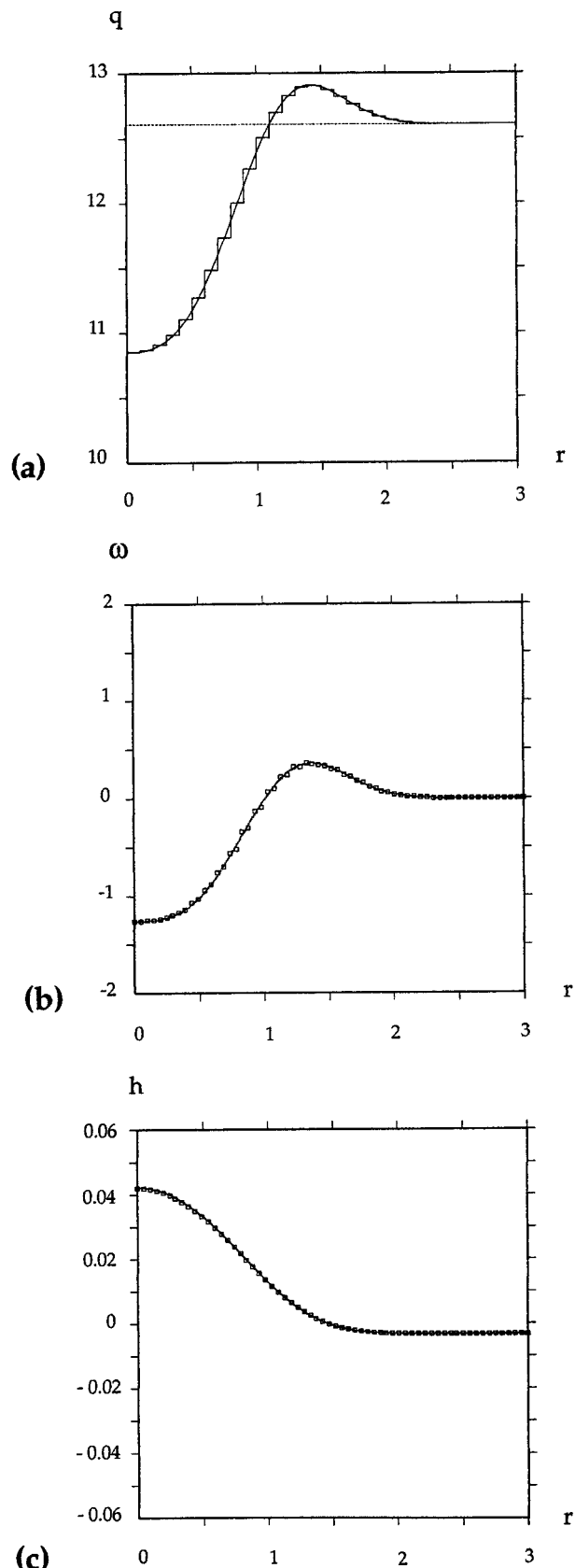
FIG. 2. Dimensionless growth rate of mode 2 [T_o is the characteristic turnover time defined by (3.1)] in the QG model as a function of the steepness parameter α for various values of Bu: 100, 4, 1, 0.44, 0.25, 0.16, 0.11. The bold line shows Bu = 1, while the dashed line Bu = 100.

3. Linear stability in the QG limit

To better understand the shallow-water simulation results, we have performed a linear stability analysis of the vortices defined by (1) in the QG limit. Using the PV discretization described in the previous section, we implemented the exact stability analysis outlined in Waugh and Dritschel (1991). The number of PV contours used to represent the continous profile was increased until the maximum growth rate converged to within 5%. We used the characteristic eddy turnover time

$$T_o = \frac{4\pi}{\omega_{max}} = \frac{4\pi}{\epsilon f_o} \qquad (3.1)$$

to rescale the growth rates obtained from the QG linear stability analysis for comparison with the CASL shallow-water simulations. Of course, QG theory is only valid for $Fr^2 \ll Ro \ll 1$. But the Burger number Bu = $(Ro/Fr)^2$ may take any value so long as Bu $\gg$ Ro. Therefore, we examine the QG stability for a wide range of Bu, on the understanding that its applicability may be restricted by the actual Rossby number.

Figure 2 shows the linear growth rate (corresponding to the most unstable mode: azimuthal mode 2) as a function of the steepness parameter α, for various values of Bu. The growth rate increases with α and with Bu. Furthermore, near marginal stability, there is a supercritical bifurcation of the form

$$\sigma \propto B(\alpha - \alpha_c) + O[(\alpha - \alpha_c)^2]. \qquad (3.2)$$

Therefore, by linear extrapolation, we can determine the critical steepness parameter α_c, shown in Fig. 3, and
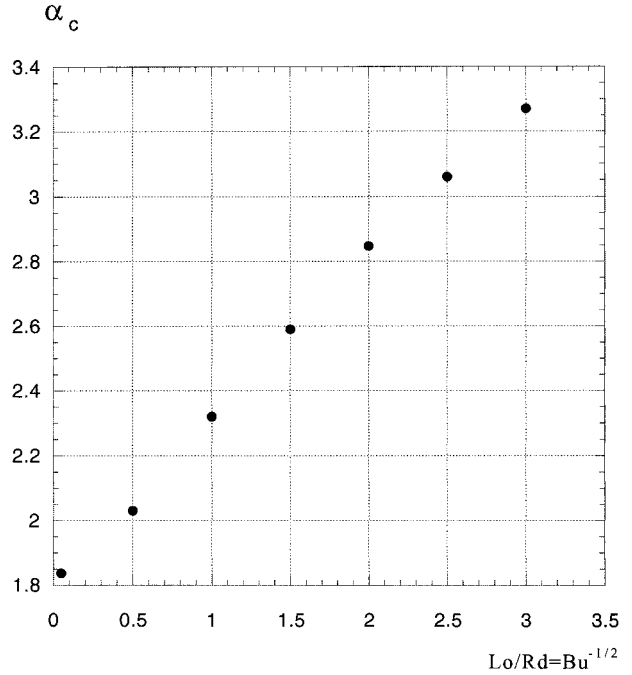
α_c

FIG. 3. Dependence of the critical steepness parameter α_c (corresponding to marginal stability) on the scale ratio $L_o/R_d = $ Bu$^{-1/2}$, in the QG model.

the parameter B, shown in Fig. 4, for various values of Bu. We recover here the general tendency indicated by the Rayleigh stability criterion, namely, that when the characteristic horizontal scale L_o increases, a wider class of vortices becomes stable. Indeed, for small vortices
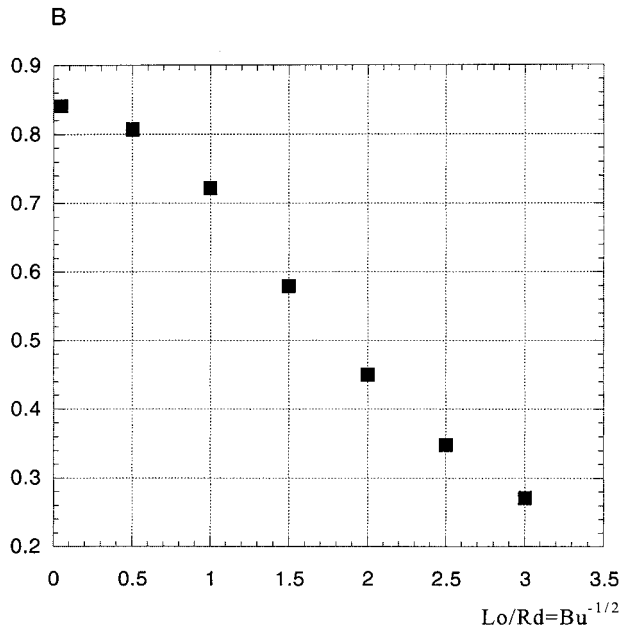
B

FIG. 4. Dependence of the parameter B [corresponding to Eq. (3.2)] on the Burger number Bu = $(R_d/L_o)^2$, in the QG model.
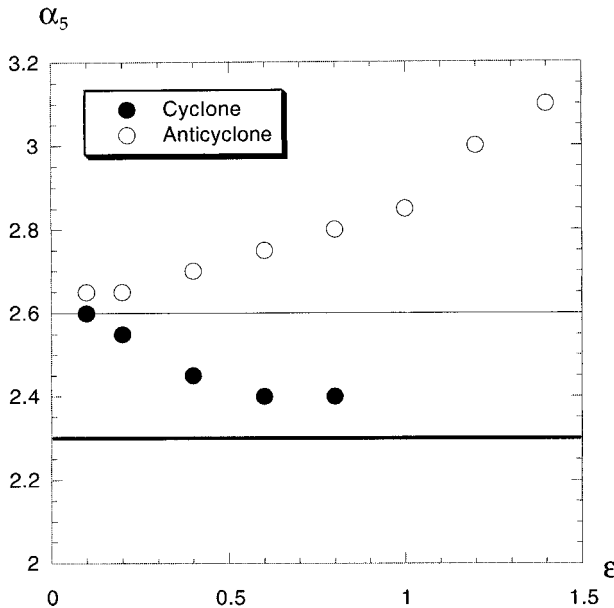
FIG. 5. Dependence of the critical value α_5 on the dynamical Rossby number for cyclones and anticyclones. The Burger number is equal to one. The thick line corresponds to the marginal stability limit $\alpha_c = 2.3$ in the QG model while the thin solid line corresponds to the α_5 value.
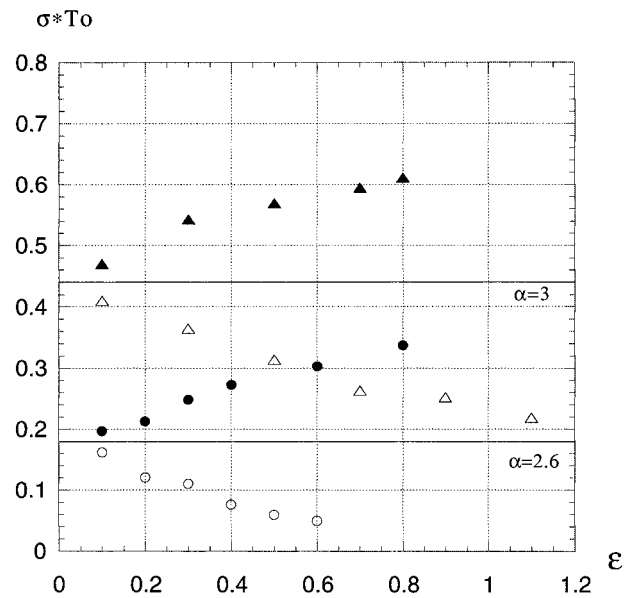

FIG. 6. Evolution of the dimensionless growth rate of mode 2 for cyclones (filled dots) and anticyclones (open dots) as a function of the dynamical Rossby number. Circles and triangles correspond to vortices having steepness parameters $\alpha = 2.6$ and $\alpha = 3$. The solid lines shows the QG growth rates.

(Bu $\gg$ 1) the PV is dominated by vorticity variations and therefore all isolated vortices are conditionally unstable, while for large vortices (Bu $\ll$ 1) the PV is dominated by height variations, and all vortices tend to be linearly stable. Note, however, that for the class of vortices defined by (1) all PV profiles are nonmonotonic; see appendix A.

Hence, according to the QG linear stability analysis:

- Vortices with broad vorticity profiles are stable while those with steep vorticity profiles tend to be unstable. The stability and therefore the lifetime is strongly sensitive to the profile.
- The behavior of cyclones and anticyclones having the same vorticity profile are identical.
- Large-scale vortices ($L_o > R_d$) are more stable than small ones ($L_o < R_d$). The growth rate decreases as the vortex size increases and the extent of the unstable region shrinks.

4. Ageostrophic effects

To estimate the influence of ageostrophic effects on vortex stability, we resorted to the numerical simulation of the shallow-water equations. The Burger number was first fixed at unity ($L_o = R_d$), while the dynamical Rossby number was increased from a very small value where geostrophic balance applies to nearly unity where gradient wind balance applies. The numerical determination of the critical steepness parameter α_c is difficult because many PV contours are needed to represent the evolution near marginal stability. We have opted instead

to approximate the marginal stability boundary by $\alpha = \alpha_5$ corresponding to the growth rate $\sigma = 1/(5T_o)$. The growth rate is determined from the temporal evolution (initial exponential growth) of azimuthal mode 2 of the vorticity field.

As shown in Fig. 5, a significant cyclone–anticyclone asymmetry emerges with increasing ε. A similar asymmetry appears in the growth rate. According to Fig. 6, when ε is small the growth rates for cyclones and anticyclones are both close to the values predicted by the QG linear stability analysis. But as ε increases, the dimensionless growth rate σT_o increases for cyclones while it decreases for anticyclones. The growth rate for a cyclone can be one order of magnitude higher than for the equivalent anticyclone (having the same velocity profile, but with opposite sign) due to ageostrophic effects. See for instance the case $\varepsilon = 0.6$ when $\alpha_c = 2.6$ in Fig. 6.

These results confirm that the dynamical Rossby number ε is the relevant parameter to quantify ageostrophic effects. Note that the standard Rossby number Ro $= V_{max}/L_o f_o$ commonly used in the analysis of observational data is, in general, two or three times smaller than the dynamical Rossby number. For the family of vortices we have studied,

$$\text{Ro} = \frac{1}{2}\varepsilon \exp\left(-\frac{1}{\alpha}\right). \qquad (4.1)$$

Hence, a value Ro $\simeq 0.25$ would correspond to a dynamical Rossby number ε close to unity (e.g., $\varepsilon = 0.8$ for a Gaussian vortex). We have also studied the non-
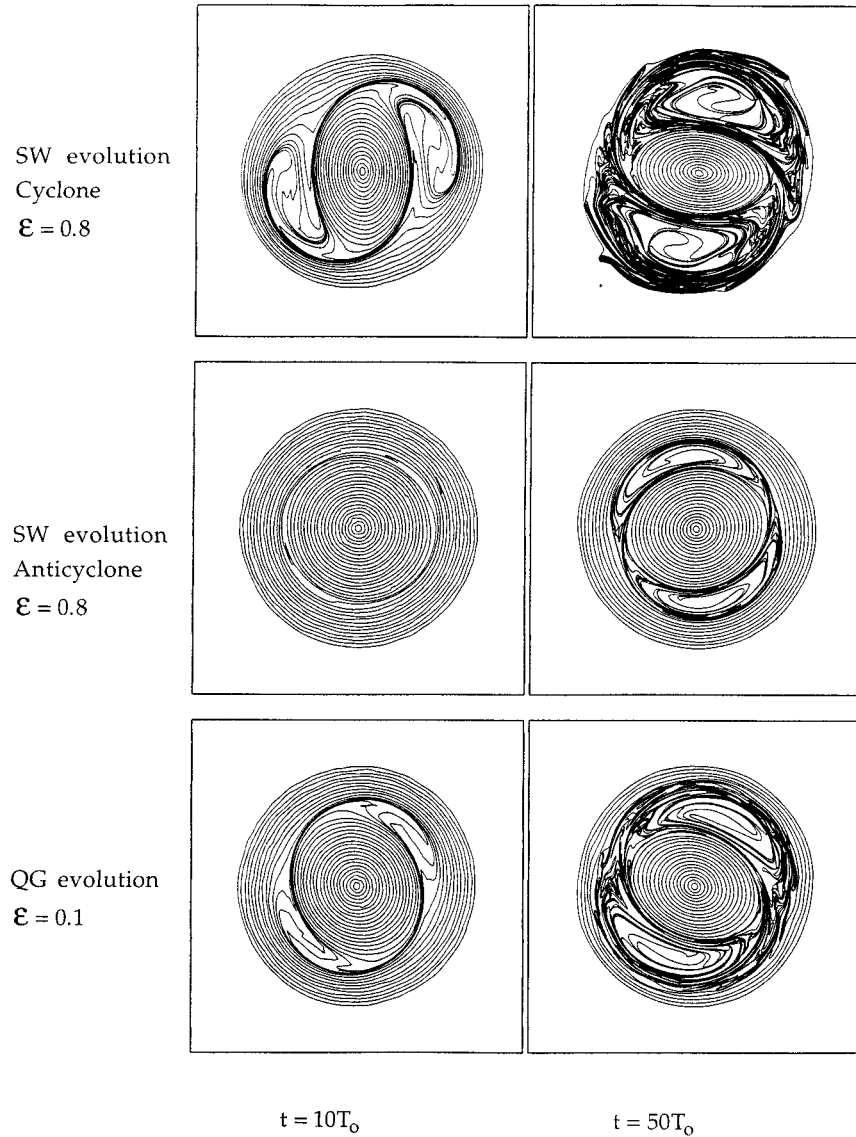
FIG. 7. Evolution of the PV contours for initially circular vortices (randomly disturbed) having Bu = 1 and a steepness parameter $\alpha = 3$. Three cases are shown: $\epsilon = 0.8$ cyclone (top), $\epsilon = 0.8$ anticyclone (middle), and $\epsilon = 0.1$ cyclone (bottom). Recall that $T_o = 4\pi/\epsilon f_o$.

linear evolution of unstable vortices having steep vorticty gradients ($\alpha = 3$) and have compared the evolution of cyclonic and anticyclonic vortices in both the QG regime ($\varepsilon = 0.1$) and a highly ageostrophic regime ($\varepsilon = 0.8$). As shown in Fig. 7, the departure from geostrophy tends to make anticyclones less unstable than cyclones. The elliptical deformation and the mixing around cyclonic vortices are pronounced; on the other hand, anticyclones remain virtually axisymmetric and coherent.

Hence, according to our numerical simulations, ageostrophic effects become significant when the dynamical Rossby number is $O(1)$, and these ageostrophic effects introduce a cyclone–anticyclone asymmetry. The

unstable region for anticyclones diminishes in the parameter space, while it expands for cyclones. The instabilities develop in fundamentally different ways as well, with anticyclones showing little disruption and cyclones showing strong deformation and vigorous mixing.

5. Large-scale effects

We next turn to the influence of large-scale effects ($L_o > R_d$) on vortices that are close to geostrophic balance ($\epsilon \ll 1$). The purpose of this investigation is to know how far we can rely on the quasigeostrophic formulation to describe the unstable evolution of isolated
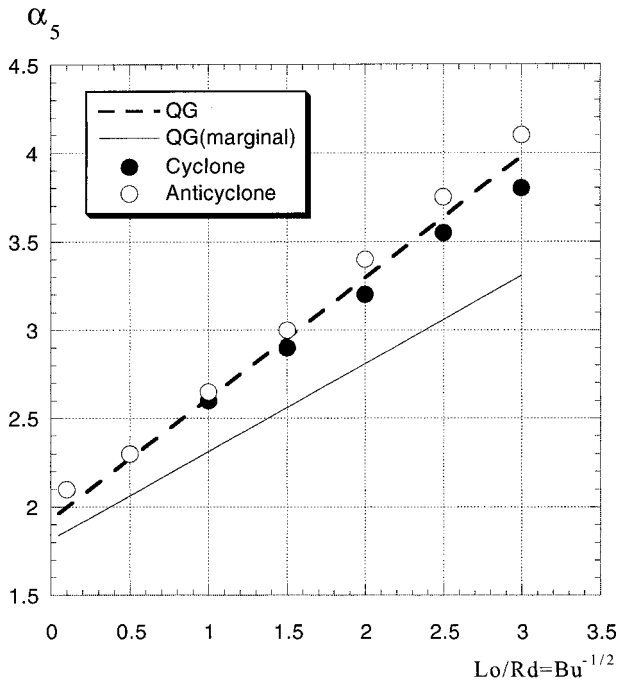
FIG. 8. Dependence of the critical value α_5 on the Burger number for cyclones and anticyclones. The Rossby number is equal to 0.1. The solid line corresponds to the marginal stability limit in the QG model while the dashed line corresponds to the α_5 value in QG.

vortices when the Burger number Bu $= (R_d/L_o)^2$ becomes small.

Figure 8 shows the dependence of the steepness parameter α_5 on L_o/R_d for cyclones and anticyclones having opposite vorticity. The main tendency is that the unstable region, for both cyclones and anticyclones, decreases in the parameter space as the Burger number decreases. In other words, a wider class of vorticity profiles are stable when the characteristic horizontal scale of the vortex is increased. The value of α_5 follows surprisingly well the prediction of the QG linear stability analysis. The stabilization of large-scale vortices is illustrated in Fig. 9 showing the nonlinear evolution of unstable vortices having a steep vorticity profile $\alpha = 4$ for three different values of Bu. The first case, Bu $= 9$, may be well described by the 2D barotropic system (Bu $\to \infty$) and leads to dipole splitting. The second case, Bu $= 1$ in the QG regime, leads to the classical tripole instability. The third case, Bu $= 0.11$ in the frontal dynamics regime, leads to a cyclone–anticyclone asymmetry. Hence, small-scale vortices are more unstable than large-scale ones. Therefore, the mixing resulting from the nonlinear evolution of unstable vortices is enhanced in the high Burger number regime ($L_o \ll R_d$).

These simulations show that large-scale vortices become more stable as the Burger number decreases. This effect is relatively well reproduced by the QG model. However, when Bu < 1, anticyclones exhibit greater stability than cyclones, and this cannot be explained using the QG model.
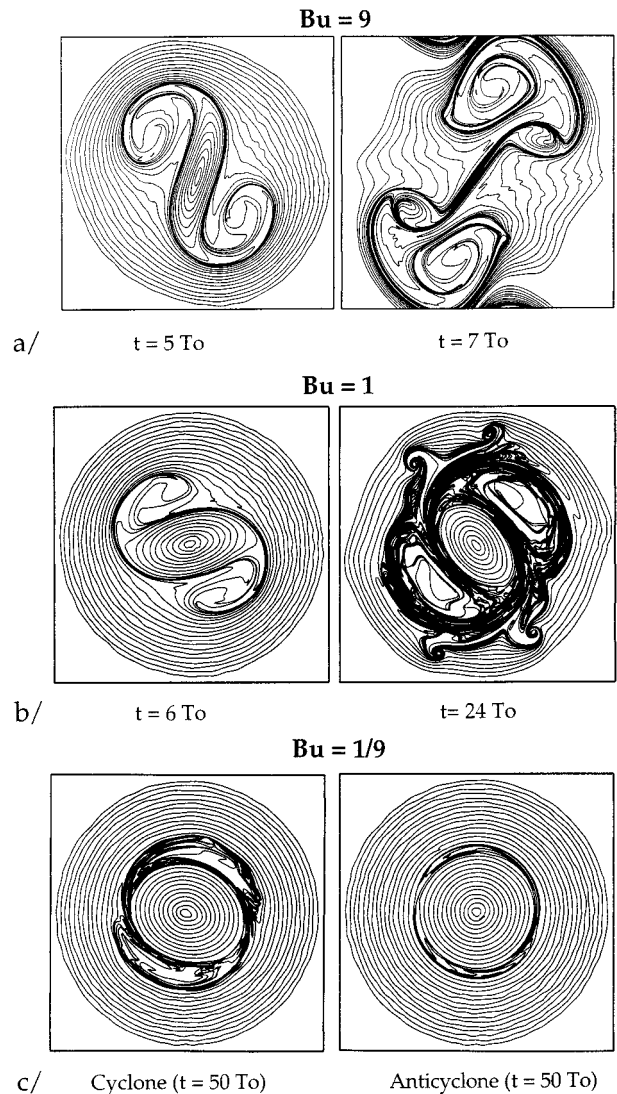

FIG. 9. Evolution of the PV contours for initially circular vortices having the same vorticity profile (steepness parameter $\alpha_c = 4$) but different Burger numbers (a) Bu $= 9$, (b) Bu $= 1$, and (c) Bu $= 0.11$. For the latter case only the final stage of the evolution is shown at $t = 50T_o$ for both the cyclonic and the anticyclonic vortices. All vortices have the same Rossby number $\epsilon = 0.1$, and therefore they are nearly in geostrophic balance.

We have also investigated the role of ageostrophic effects in the evolution of small and large-scale vortices (Fig. 10). The relative deviation of the growth rate of the most unstable mode (wave 2) from the standard QG analysis gives a quantitative estimate of these effects. We have shown that when the Burger number decreases, ageostrophic effects become more important. For an anticyclonic vortex having a dynamical Rossby number $\varepsilon = 0.3$, the deviation of the growth rate increases from 7% to 50% when the Burger number decreases from 4 to 0.44. As expected, a significant departure from QG dynamics will occur when the relative amplitude of the height field h/H_o (or the ratio ε/Bu) approaches unity.
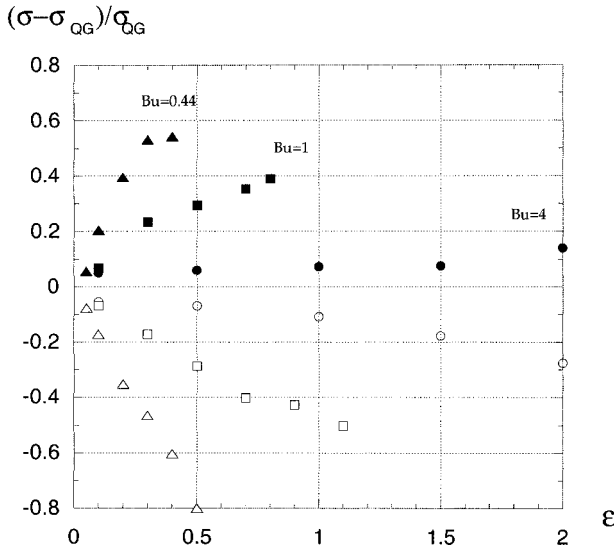
$(\sigma - \sigma_{QG})/\sigma_{QG}$

FIG. 10. The relative deviation of the growth rate from a standard QG analysis for several values of the Burger number, for both cyclones (filled dots) and anticyclones (open dots), and for various values of the Rossby number ϵ. Key: Bu = 0.44 (triangles), Bu = 1 (squares), and Bu = 4 (circles). All the vortices have the same velocity profile corresponding to a steepness parameter $\alpha = 3$.

FIG. 11. Evolution of the PV contours for initially circular vortices having a steepness $\alpha = 3$, a characteristic scale 1.5 times larger than the deformation radius (Bu = 0.44), and a dynamical Rossby number $\epsilon = 0.3$.

Hence, the asymmetry arises from a combination of both large-scale and ageostrophic effects as emphasized in Fig. 11. Significant differences in the evolution of cyclones and anticyclones may occur even if the dynamical Rossby number is still relatively small, for example, $\varepsilon = 0.3$, and the vortex size is just 1.5 times larger than the deformation radius (i.e., Bu = 0.44).

6. A quantitative law for cyclone–anticyclone asymmetry

According to the numerical results of Polvani et al. (1994) for decaying shallow water turbulence, the cyclone–anticyclone asymmetry seems to be controlled by a single parameter. Indeed, they have shown that the skewness of vorticity (initially zero) always becomes negative. This value increases with the Froude number $Fr = \epsilon/\sqrt{Bu}$. However, Arai and Yamagata (1994) have shown that the difference in stability between elliptical cyclones and anticyclones (at a constant Froude number) is strongly influenced by the relative deviation of the height field (ϵ/Bu). If we assume that the normal mode instability, which grows slowly compared to inertia–gravity wave frequency, is controlled by the PV, then one would expect the cyclone–anticyclone asymmetry to be induced by the non-QG part of the PV. In fact, this first-order correction to the QG PV is of order ϵ/Bu. In appendix B, it is shown that this nonlinear correction increases the PV gradient in the vortex core for cyclones but decreases it for anticyclones.

For our results, the rescaling of $(\sigma - \sigma_{QG})/\sigma_{QG}$ (deviation from QG of the most unstable growth rate) with
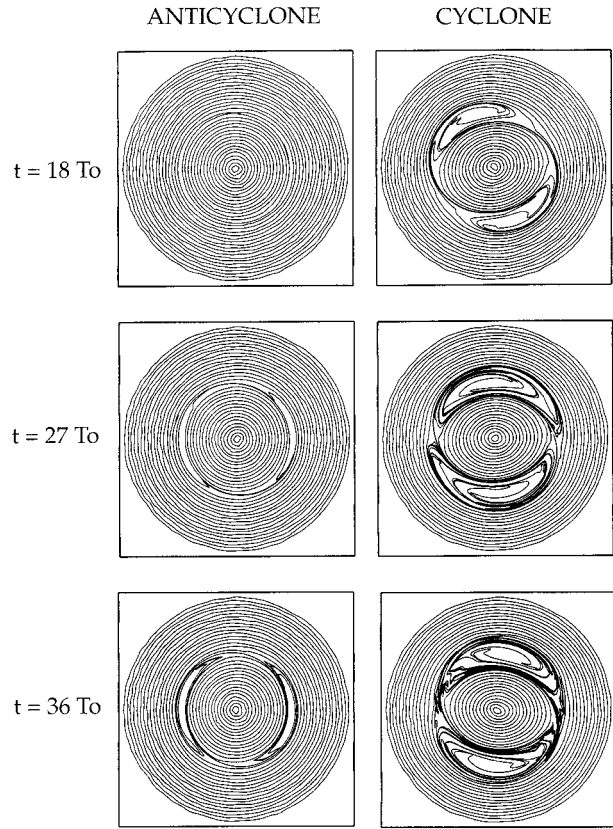
ϵ/Bu (see Fig. 12) or $\epsilon/\sqrt{Bu}$ does not give a satisfactory relation. However, we have found that, for a given steepness α, the growth rates rescale surprisingly well with

$$(\sigma - \sigma_{QG})/\sigma_{QG} \propto \epsilon/(Bu - Bu_c), \qquad (6.1)$$

where Bu_c is the critical Burger number corresponding to the QG marginal stability of the given vorticity profile. The value of $Bu_c = Bu(\alpha = \alpha_c)$ can be directly extracted from Fig. 3. The relation (6.1) was verified over a wide region of the (ϵ, Bu) parameter space for two vorticity profiles $\alpha = 3$ ($Bu_c = 0.17$) and $\alpha = 2.6$ ($Bu_c = 0.44$), shown respectively in Figs. 13a and 13b. One may verify from these figures that the proportionality coefficient in (6.1) is of order unity, differing only slightly between the $\alpha = 3$ and $\alpha = 2.6$ profiles.

Hence, according to relation (6.1), if a vorticity profile is far from its marginal stability in QG (Bu $\gg$ Bu$_c$), the difference in lifetime between cyclones and anticyclones is controlled by a single parameter: the relative amplitude of the height field ϵ/Bu. On the other hand, for vortices close to QG marginal stability (Bu $\cong$ Bu$_c$) a strong asymmetry may occur even if the surface deviation remains small. Then, a significant deviation from QG dynamics may occur even if $Fr^2 \ll \epsilon \ll 1$. In fact,

the characteristic evolution time for an unstable vortex close to marginal stability is very long $O(\epsilon^{-1})$ and the asymptotic expansion leading, at the first order, to the QG model is not formally valid for such timescales. Higher-order nonlinearity needs to be taken into account in a multiple-time scale analysis. Such nonlinearity is likely to explain the breaking of symmetry between cyclones and anticyclones near QG marginal stability.

7. Significance

Several key questions arise from this research. First of all, is it possible to observe in nature mesoscale eddies in a range of parameters where ageostrophic or large-scale effects are significant? If so, do these eddies exhibit a cyclone–anticyclone asymmetry?

Isolated vortices are more common in the oceans than in the Earth's atmosphere or in other planets where strong environmental shear and diabatic effects may play important roles. While a reliable horizontal scale L_o of vortices can be extracted from ocean data, similarly reliable velocity profiles and estimates of the local deformation radius R_d are difficult to obtain. Usually, the maximum of the velocity profile is used in order to estimate the standard Rossby number $\text{Ro} = V_{\max}/L_o f_o$ of the vortex. As mentioned above, the dynamical Rossby number ϵ may be two to three times larger than Ro depending on the velocity profile. The deformation radius corresponding to an equivalent 1½ shallow-water layer model can be estimated from isopycnal displacements (Olson 1985). According to the large dataset analyzed by Olson (1991) a great variety of vortices are observed having a wide range of characteristics (see Fig. 14). Agulhas eddies have characteristic horizontal scales two or three times larger than the deformation radius (small Burger number) while Gulf Stream rings may have a moderate Rossby number. Both large-scale cyclones and anticyclones are generated from the meandering of strong oceanic currents. No evident asymmetry appears in the distribution of vortices even though the longest-lived structures observed are anticyclonic (Olson 1991). However, an asymmetry in the shape of eddies formed behind Gran Canaria Island was recently observed (Aristegui et al. 1994). According to these authors, the elliptical deformation of the cyclonic vortices is more pronounced than that for the anticyclonic ones. Assuming that the mechanism of eddy generation in this case is analogous to the von Kármán vortex street instability, eddies with moderate Rossby number are likely to appear. Hence, the observed asymmetry could be a manifestation of the ageostrophic effects mentioned in this paper. Note however, that a nontrivial vertical structure of the flow could also be responsible for the observed asymmetry.

Another question arises about the importance of 3D instability neglected in the shallow-water treatment of this problem. It is well known that ageostrophic anticyclonic vortices may be subject to inertial instability
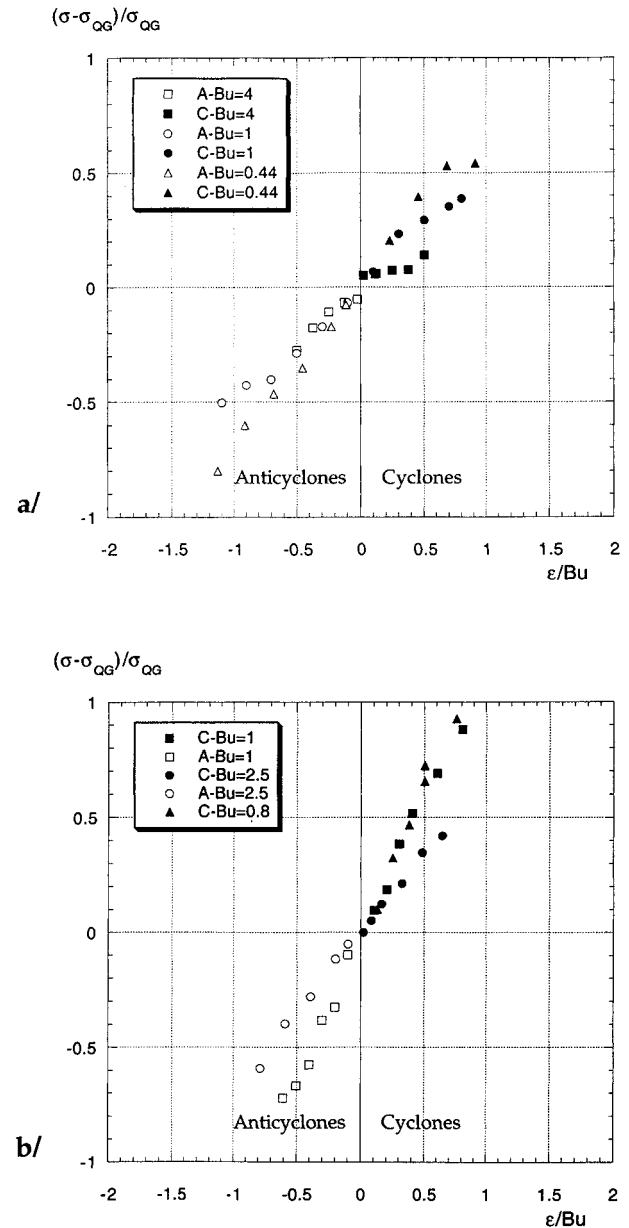

FIG. 12. Deviation of the growth rates from a standard QG analysis as a function of ϵ/Bu. Values are plotted for various cyclonic ($\epsilon > 0$) and anticyclonic ($\epsilon < 0$) vortices having a steepness (a) $\alpha = 3$ and (b) $\alpha = 2.6$.

(also called centrifugal instability). How does this 3D instability compete with the 2D ageostrophic stabilization described in the present paper?

According to the extended Rayleigh criterion for centrifugal instability (Kloosterziel and van Heijst 1991; Mutabazi et al. 1992) all circular anticyclonic vortex columns will be unstable to vertical perturbations when the dynamical Rossby number ϵ is larger than one (i.e., for $q < 0$). In this case there is an annular region surrounding the core where the Rayleigh discriminant is negative. Isolated cyclonic vortices may also become
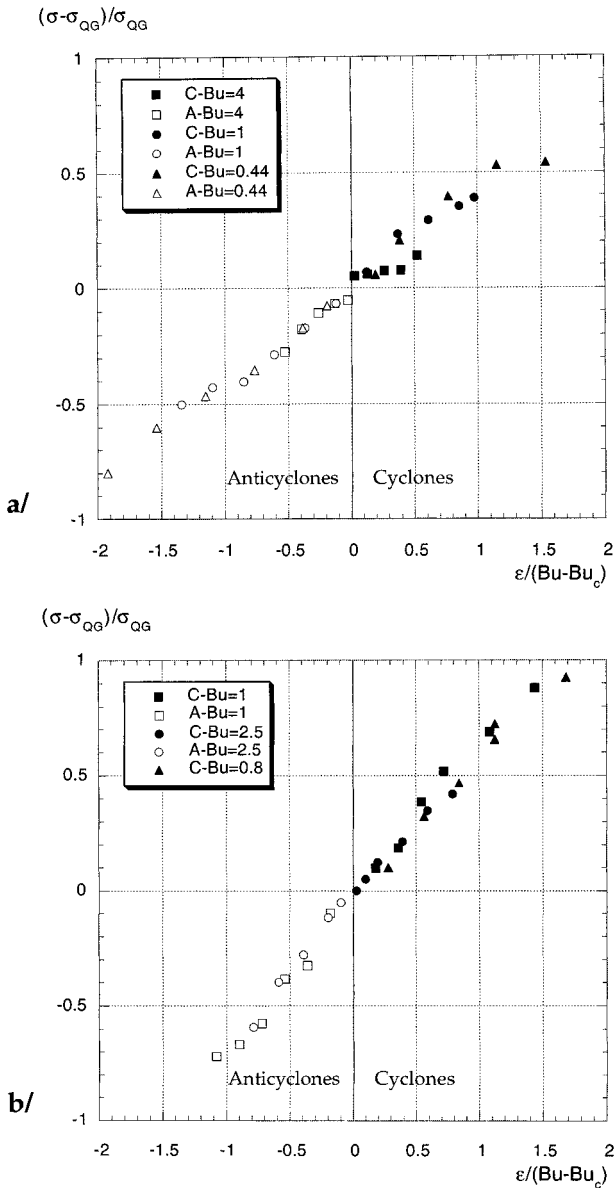
a/

FIG. 14. Distribution of vortices generated by oceanic currents (Gulf Stream, Kuroshio, Algulhas), from Olson (1991).

b/

FIG. 13. Same notation as Fig. 12. Deviation of the growth rates from a standard QG analysis as a function of $\epsilon/(Bu - Bu_c)$; Bu_c is the critical Burger number, obtained from the QG stability analysis (Fig. 3): $Bu_c = 0.17$ for $\alpha = 3$ and $Bu_c = 0.44$ for $\alpha_c = 2.6$.

ample, $\epsilon \cong 6$ for the circular vortex patch (Potylitsin and Peltier 1998). Moreover, stratification tends to reduce growth rate (Potylitsin and Peltier 1998). Finally, the vortices modeled by the shallow-water system are not barotropic, and their actual 3D structure may give rise to added stability. It is then possible that anticyclonic vortices may survive for Rossby numbers significantly larger than unity.

One of the main concerns about using the reduced-gravity model is its trivialization of the vertical flow structure. In order to better understand oceanic observations, an active lower layer should be taken into account. In this case, how is the baroclinic instability expected to change the results obtained and how could it affect the cyclone–anticyclone asymmetry?

It is well known that the influence of Bu on the stability of QG vortices is sensitive to the presence of an active lower layer. Indeed, unlike the one-layer case, vortices become increasingly unstable when Bu decreases in a two-layer QG model (Ikeda 1981). However, it may still be possible to obtain stable vortices with length scales larger than the deformation radius if the initial steady state has a corotating deep-layer flow. Linear stability analyses performed by Helfrich and Send (1988) and Flierl (1988) have shown that a corotating lower layer reduces the growth rate of unstable QG vortices, while a counterrotating lower layer enhances it. Besides, the departure from QG appears to amplify this behavior. For a two-layer shallow-water model, the normal modes of instability disappear for both warm (anticyclonic) and cold (cyclonic) large-scale eddies (Bu ≪ 1) having a weak corotaing flow (Dewar and Killworth 1995; Killworth et al. 1997). As far as the cyclone–anticyclone asymmetry is concerned, recent nu-

inertially unstable, but this occurs for a higher value of the Rossby number depending on the vorticity profile. This instability has been observed in laboratory experiments (Kloosterziel and van Heijst 1991; P. Bonneton 1998, personal communication) and in 3D numerical simulations (Bartello et al. 1994). Hence, in nature, one would expect ageostrophic stabilization of anticyclones only for Rossby numbers close to, but not larger than, unity. One might expect an even greater range of applicability, given that the instability is weak for ϵ slightly greater than unity and that maximum instablity occurs for much higher dynamical Rossby numbers; for ex-
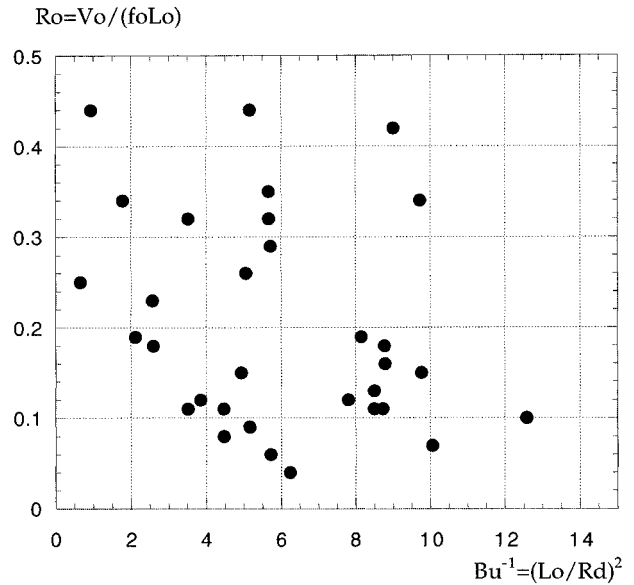
merical simulations in a two-layer fluid (Benilov et al. 1998) have shown that among various eddies having Gaussian profiles, only some anticyclonic ageostrophic vortices ($\epsilon \gtrsim 0.6$) are stable. Hence, the ageostrophic stabilization presented in section 6 could still be an efficient mechanism for a stratified 3D flow.

8. Conclusions

By means of high-resolution shallow-water simulations, conducted using the recently developed CASL algorithm (Dritschel et al. 1999), we have examined the stability and nonlinear evolution of isolated vortices as a function of their shape, size, and strength. The evolution of each cyclone was compared to its equivalent anticyclone: a vortex having the same vorticity profile but with opposite sign. It has been shown, for this 1½-layer model, that a significant departure from quasigeostrophic dynamics occurs when the ratio of the dynamical Rossby number to the Burger numer ϵ/Bu is $O(1)$ or when vortices are close to marginal stability in QG. In all cases, this departure is characterized by a cyclone–anticyclone asymmetry, which is opposite to the well-known asymmetry induced by three-dimensional inertial instability on vortex columns. Indeed, both ageostrophic ($\epsilon \cong 1$) and large-scale effects (Bu $\ll 1$) tend to destabilize cyclonic vortices and stabilize anticyclonic ones. This asymmetry appears to be significant over the range of parameters characterizing isolated vortices in the ocean, and may therefore explain the greater observed longevity of anticyclones there. However, to fully reproduce the asymmetry of the oceanic observations, the three-dimensional structure of the flow should be taken into account.

APPENDIX A

Asymptotic Limit of the PV Gradient

Using the dynamical Rossby number ϵ and the relative amplitude of the height field $\lambda = \epsilon$/Bu the dimensionless PV may be expressed as

$$q = \frac{1 + \epsilon\omega(s)}{1 + \lambda h(s)} \qquad (A.1)$$

and its dimensionless gradient as

$$\partial_s q = \frac{1}{1 + \lambda h(s)}(\epsilon\partial_s\omega - \lambda q\partial_s h). \qquad (A.2)$$

Close to the vortex center, the PV gradient of a cyclone is always negative. If this cyclone satisfies (1), the asymptotic limit for large s ($s \to \infty$) gives

$$\partial_s\omega \to \frac{s^{2\alpha-1}}{2}\exp\left(-\frac{s^\alpha}{\alpha}\right) \qquad (A.3)$$

$$\partial_s h = v + \epsilon\frac{v^2}{s} \to \frac{1}{2}s\exp\left(-\frac{s^\alpha}{\alpha}\right), \qquad (A.4)$$

therefore

$$\partial_s q \to (\epsilon s^{2(s-1)} - \lambda)\frac{s}{2(1 + \lambda h)}\exp\left(-\frac{s^\alpha}{\alpha}\right). \qquad (A.5)$$

If the steepness parameter satisfies $\alpha > 1$, for any values of (ϵ, Bu) the PV gradient will tend to a positive value for large s. Similar results with opposite signs are obtained for anticyclones. Hence, all vortices defined by (A.1) have a nonmonotonic PV profile.

APPENDIX B

First-Order Correction of the PV Gradient

Using the dimensionless parameters (ϵ, λ), introduced in appendix A, we derive the first-order correction of the PV gradient from the standard QG regime where $\lambda \ll 1$ and $\epsilon \ll 1$. From (A.2) and using the dimensionless formulation of the gradient wind balance,

$$\partial_s h = v + \epsilon\frac{v^2}{s}, \qquad (B.1)$$

we get

$$\partial_s q = \epsilon\left[\partial_s q_{QG} - \lambda\left(\partial_s(h_{QG}q_{QG}) + \frac{v^2}{s}\right)\right] + O(\epsilon^2\lambda, \epsilon\lambda^2), \qquad (B.2)$$

where q_{QG} and h_{QG} are defined by

$$q_{QG} = \omega - \frac{1}{Bu}h_{QG} \qquad (B.3)$$

$$\partial_s h_{QG} = v. \qquad (B.4)$$

Hence, the first-order correction of the PV gradient scales as $\lambda = \epsilon$/Bu. In the center of the vortex where $\partial_s(h_{QG}q_{QG}) \geq 0$ this nonlinear correction is positive for both cyclones and anticyclones; therefore it increases the PV gradient of cyclones and decreases that of anticyclones.

REFERENCES

Arai, M., and T. Yamagata, 1994: Asymmetric evolution of eddies in rotating shallow water. *Chaos,* **4** (2), 163–175.

Aristegui, J., P. Sangra, S. Hernandez-Leon, M. Canton, A. Hernandez-Guerra, and J. L. Kerling, 1994: Island-induced eddies in the Canary Islands. *Deep-Sea Res.,* **41,** 1509–1525.

Arnold, V. I., 1978: *Mathematical Methods of Classical Mechanics.* Springer-Verlag, 462 pp.

Bartello, P., O. Metais, and M. Lesieur, 1994: Coherent structures in rotating three-dimensional turbulence. *J. Fluid Mech.,* **273,** 1–29.

Benilov, E. S., and Coauthors, 1998: On the stability of large-amplitude vortices in a continuously stratified fluid on the f-plane. *J. Fluid Mech.,* **355,** 139–162.

Ben Jelloul, M., and V. Zeitlin 1999: Remarks on stability of the rotating shallow-water vortices in the frontal dynamics regime. *Nuovo Cimento Soc. Ital. Fis. C,* **22,** 931–941.

Carton, X., and B. Legras, 1994: The life-cycle of tripoles in two-dimensional incompressible flows. *J. Fluid Mech.,* **267,** 53–82.

——, C. R. Flierl, and L. Polvani, 1989: The generation of tripoles from unstable axisymmetric isolated vortex structure. *Europhys. Lett.,* **9,** 339–344.

Cushman-Roisin, B., 1986: Frontal geostrophic dynamics. *J. Phys. Oceanogr.,* **16,** 132–143.

Dewar, W. K., and P. D. Killworth, 1995: On the stability of oceanic rings. *J. Phys. Oceanogr.,* **25,** 1467–1487.

Dritschel, D. G., and M. H. P. Ambaum, 1997: A contour-advective semi-Lagrangian numerical algorithm for simulating fine-scale conservative dynamical fields. *Quart. J. Roy. Meteor. Soc.,* **123,** 1097–1130.

——, L. M. Polvani, and A. R. Mohebalhojeh, 1999: The contour-advective semi-Lagrangian method for the shallow water equations. *Mon. Wea. Rev.,* **127,** 1551–1565.

Flierl, G. R., 1988: On the instability of geostrophic vortices. *J. Fluid Mech.,* **197,** 349–388.

Helfrich, K. R., and U. Send, 1988: Finite-amplitude evolution of two-layer geostrophic vortices. *J. Fluid Mech.,* **197,** 331–348.

Holm, D. D., J. E. Mardsen, T. Ratiu, and A. Weinstein, 1985: Non-linear stability of fluid and plasma equilibria. *Phys. Rep.,* **123,** 1–116.

Ikeda, M., 1981: Instability and splitting of mesoscale rings using a two-layer quasigeostrophic model on an *f*-plane. *J. Phys. Oceanogr.,* **11,** 987–998.

Killworth, P. D., J. R. Blundell, and W. K. Dewar, 1997: Primitive equation instability of wide oceanic rings. Part I: Linear theory. *J. Phys. Oceanogr.,* **27,** 941–962.

Kloosterziel, R. C., and C. J. F. van Heijst, 1991: An experimental study of unstable barotropic vortices in a rotating fluid. *J. Fluid Mech.,* **223,** 1–124.

Mutabazi, I., C. Normand, and J. E. Wesfreid, 1992: Gap size effects on centrifugally and rotationally driven instability. *Phys. Fluids A,* **4,** 1199–1205.

Olson, D. B., 1985: Two-layer diagnostic model of the long-term physical evolution of warm-core ring 82B. *J. Geophys. Res.,* **90,** 8813–8822.

——, 1991: Rings in the ocean. *Annu. Rev. Planet. Sci.,* **19,** 283–311.

——, and R. J. Evans, 1986: Rings of the Agulhas. *Deep-Sea Res.,* **33,** 27–42.

Orlandi, P., and G. J. F. van Heijst, 1992: Numerical simulations of tripolar vortices in 2D flows. *Fluid Dyn. Res.,* **9,** 179–206.

Pedlosky, J., 1987: *Geophysical Fluid Dynamics.* Springer-Verlag, 710 pp.

Polvani, L. M., J. C., McWilliams, M. A. Spall, and R. Ford, 1994: The coherent structures of shallow water turbulence: Deformation-radius effects, cyclone–anticyclone asymmetry, and gravity-wave generation. *Chaos,* **4** (2), 177–186.

Potylitsin, P. G., and W. R. Peltier, 1998: Stratification effects on the stability of columnar vortices on the f-plane. *J. Fluid Mech.,* **355,** 45–79.

Ripa, P., 1987: On the stability of elliptical vortex solutions of the shallow water equations. *J. Fluid Mech.,* **183,** 343–363.

Smith, B. A., and Coauthors, 1979: The Jupiter system through the eyes of Voyager 1. *Science,* **204,** 951–972.

Waugh, D. W., and D. G. Dritschel, 1991: The stability of filamentary vorticity in two-dimensional geophysical vortex-dynamics models. *J. Fluid Mech.,* **231,** 575–598.